DESIGN OF THE PHASING TRAJECTORY FROM A LOW LUNAR ORBIT TO NEAR RECTILINEAR HALO ORBIT

Giordana Bucchioni [*], and Mario Innocenti[†]

The paper presents three different approaches to the design of a phasing trajectory in a cislunar environment, where the third body perturbation is considered non-negligible. The working framework is the one proposed by the ESA's Heracles mission in witch the passive target spacecraft -LOP-G- is orbiting on a Near Rectilinear Halo Orbit and the Lunar Ascent Element must reach that orbit from a Low Lunar Parking Orbit to start the rendezvous procedure. In this scenario the authors propose three different ways to design such phasing manoeuvre under the Circular Restricted Three Body Problem hypotheses: Lambert/Differential correction, Hohmann/Differential correction and Optimization. The three approaches are compared in therms of ΔV consumption, accuracy and time of flight. Finally, a selected solution is also validated under the Restricted Elliptic Three Body Problem Hypotheses.

INTRODUCTION

The 50^{th} anniversary on the Human Moon landing has compounded an already new interest in Moon's missions. In fact many international space agencies decided to collaborate to build an orbiting space station on a Near Rectilinear Halo Orbit around the Moon to be used as base for different challenging missions within the Moon surface exploration and permanent return. A key phase of these missions is the phasing part, where the spacecraft must raise towards the orbiting space station to accomplish the rendezvous. In a cislunar environment the design of this manoeuvre is even more complex because of the presence of the third body perturbation, since both the gravity of the Moon and the Earth are non-negligible.

Phasing trajectories are manoeuvres that change the size of an original orbit in order to meet a final orbit properties at a different point in time. They are part of what we call "orbit transfer", and they can be calculated according to a large variety of specifications such as minimum ΔV, specific time interval for the transfer, etc. The computation complexity of phasing is strictly related to the dynamic model used in a fashion similar to trajectory design. The level of complexity depends also on an in-plane or out-of-plane computation outcome, and on a two-body or multiple body gravitational field hypothesis.

Depending on the mission, there are three main approaches to perform the phasing manoeuvre, which can be found in the literature, and used for actual flight implementation.

The first is based on the Lambert's problem solution. This approach relies primarily on the hypotheses of Keplerian orbits and 2 body problem, and computes a suitable orbit given initial position, final position and time of flight [1]. Lambert's approach has been proposed in the case of three-body problem as well, but lacks of analytical solution. Reference [2] uses Hill's approximation of the CR3BP applied to several mission scenarios of transfers between Earth and Lagrange points, including target Halo orbits. However only numerical complex solutions are possible with a potential high fuel expenditure. Nevertheless, the use of Lambert's approach could be useful in order to determine a first guess departing trajectory from the assumed lunar LLO orbit, since the Moon's gravity can be considered dominant over the Earth's gravity for altitudes up to 500 Km [3].

Another approach is the one proposed by Shang and co-workers [4]. A low thrust manoeuvre computation is solved via optimal control, with a cost function dependent on the power consumption and on the time of

[*] PhD candidate, Department of Information Engineering, University of Pisa, Largo Lucio Lazzarino 2, 56122, Pisa (PI), Italy
[†] Full Professor, Department of Information Engineering, University of Pisa, Largo Lucio Lazzarino 2, 56122, Pisa (PI), Italy

travel. Although not strictly applicable to our problem, it provides an example of viable numerical optimisation (using a shooting method and sequential quadratic programming).
Of more interest for the present work is the literature based on the application of manifolds theory [5] to phasing. The common denominator in these works being a target Halo or NRHO orbit, a ballistic or indirect transfer sequence following selected manifolds, time of flight requirements, and fuel expenditure.
Reference [6] reviews the CR3BP dynamics, and invariant manifolds computation. Then the connection between manifolds is addressed, and the study is applied to far rendezvous and close rendezvous using intermediate Halo orbits. In [7], the authors present a somewhat similar summary study, comparing, in terms of ΔV, a ballistic direct transfer from LLO to NRHO with a transfer using an intermediate NRHO, which could be used also for status assessment. Although there is no theoretical basis for the selection of the type and number of intermediate orbits (which is left to the mission design phase), a reduction in ΔV is achieved, especially if there are no stringent constraints on the TOF. A simulation-based stochastic analysis of fuel consumption and location and duration of a transfer correction manoeuvre is presented by the same authors in [3]. An interesting preliminary analysis of phasing, which includes safety considerations, is presented in [8]. Here the authors present the problem of safe phasing, by testing the accuracy of CR3BP motion with an Ephemeris model and parametrizing the results with respect to the degree of "out-of-plane" component of the target halo orbit. (Recall that *Halo orbits exist as a bifurcation of the planar Lyapunov orbits associated with L1 and L2 equilibria* [5]).
An additional application of manifolds theory to phasing can be found in [9]. In their paper, the authors refine the computation of the target NRHO using a Bi-Circular model, they analyze the results with a Montecarlo simulation, and they apply their method to an Earth to Moon transfer. Reference [10] presents a comparative transfer sequence to different NRHOs in terms of ΔV for trajectories computed using Lambert's arc and intermediate Halo.
The present work focuses on the phasing trajectory defined within the HERACLES mission, in particular it presents three different ways of designing the transfer trajectory from the Moon towards the Lunar Space Gateway NRHO and compares them. The paper first introduces the working scenario with the description of the equations of motion used to model the system, then it describes the three approaches and resulting trajectories, followed by an example of validation of the obtained trajectory with a more complex model, to conclude with a exhaustive comparison of the obtained results and some comments.

SCENARIO DESCRIPTION

This section reviews the models used, the assumptions made, and defines the specifics of the mission scenario considered for the design of a phasing trajectory. The boundary conditions were specified earlier and they will be repeated here for clarity's sake.
The proposed scenario is motivated by the Heracles mission of the European Space Agency (ESA), this mission has the goal of proving advancements in autonomous operations in space. The mission consists on an independent landing on the south pole of the Moon, autonomously collect some samples of the lunar surface and then bring these samples to the Lunar Space Gateway. One of the key phases of this mission is the phasing procedure from a Low Lunar Orbit to the the L2-NRHO to bring back these samples to the orbiting station. In this phase the Lunar Ascent Element (LAE) - chaser - with the samples must use ΔV changes to safely reach the target -LOP-G.

Reference Frames

To better understand the equations developed in this paper, we consider the following reference systems used in the representation of the dynamics:

- **Inertial Reference Frame**: all inertial coordinate frames have their axes aligned with the axis as defined for the Jet Propulsion Laboratory (JPL) DE2000 Ephemeris files. The x-axis points in the direction of the vernal equinox at midday of the 1st of January 2000. The z-axis points in the direction normal to the mean equatorial plane, in the direction of the North pole, while the y-axis supplements

the set to be a right-hand coordinate system. The center of the inertial frame can be located in the center of a celestial body or in the barycenter of a system of celestial bodies.

- **Synodic (Co-rotating) Reference Frame**: very suitable coordinate frames for the illustration and treatment of libration point orbits are co-rotating coordinate frames. The x-axis points from the primary body to the secondary body, the z-axis is the axis of the angular velocity of the bodies and is therefore normal to the orbital plane of the two primaries and the y-axis supplements the coordinate system to be a right-hand system, it can be centred on the secondary centre or on the system's barycenter.

Departure and Arrival Orbits

The boundary conditions for the problem refer to the chaser's departing orbit, target's orbit, and location of the insertion point for the beginning of the rendezvous phase [11].
The initial orbit is a circular LLO, with an altitude of 100 Km, and a 90 degree of inclination (polar orbit). Assuming perfect two-body dynamics, the chaser speed is V = 1.634 km/s and the orbital period is T = 1.9613 hours. The orbit is schematically shown in Figure 1. The target orbit is a L2 southern near rectilinear halo

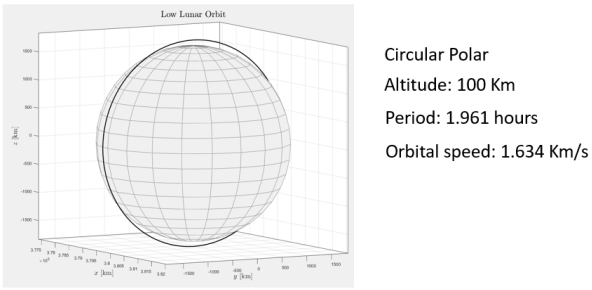

Figure 1: Reference Low Lunar Orbit

orbit shown in Figure 2. The plot on the left is the orbit's propagation using CR3BP, the graph on the right shows the orbit propagated for one year using the Ephemeris model described in Table 1.

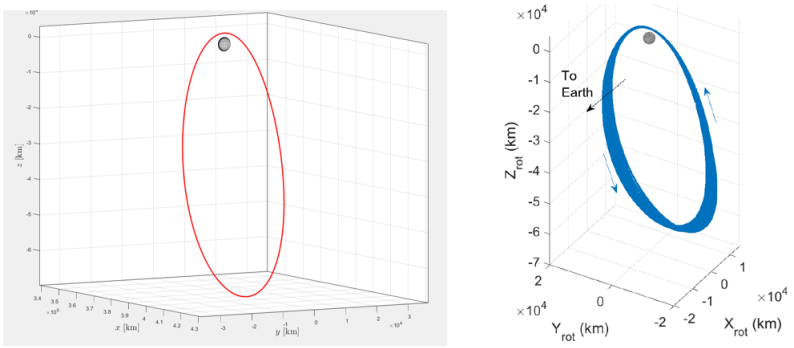

Figure 2: NRHO Target Orbit in the Synodic Frame

Equations of Motion

The equations of motion used to describe the phasing part of the LAE trajectory are based on the CR3BP model. The gravitational field is generated by two large masses (in our case the primary is the Earth, and the secondary is the Moon), moving in a planar circular motion about their common center of mass. The spacecraft are considered massless.

Table 1: Ephemeris Data for Target NRHO Propagation ESA JD2025

Information	**Data**
Comment	LOP-G Southern NRHO 9:2 Resonance
Originator	FreeFlyer (AI-SOLUTION)
Object Name	LOP-G
Center Name	Moon
Start Time	2020-01-09T00:21:00.000
Stop Time	2020-02-07T03:21:00.000
Period	6.56 days
Periselene	1,500 Km
Aposelene	70,000 Km

The CR3BP model is very convenient for preliminary trajectory design, and allows the computation of manifolds, if needed, for moving during phasing . The dynamic model is given by Eq. (1). The governing equations are repeated here for clarity's sake using the Synodic frame as reference system:

$$\dot{\mathbf{x}} = \mathbf{f}(\mathbf{x}(t)) \tag{1}$$

$$\begin{aligned} \ddot{x} - 2\dot{y} &= -\frac{\partial \bar{U}}{\partial x} \\ \ddot{y} + 2\dot{x} &= -\frac{\partial \bar{U}}{\partial y} \\ \ddot{z} &= -\frac{\partial \bar{U}}{\partial z} \end{aligned} \tag{2}$$

where the effective or augmented potential function of the system $\bar{U}(x, y, z)$ is:

$$\bar{U}(x, y, z) = -\frac{1}{2}(x^2 + y^2) + U(x, y, z) \tag{3}$$

It is possible to use a differential correction method to find the desired periodic NRHO orbit, and then to compute the invariant manifolds that take the spacecraft from its initial LLO orbit to the target orbit. The technique is used to compute the best periodic approximation of the target orbit under the Circular Restricted Three Body problem hypotheses: starting from an initial guess, the initial state is constantly corrected inverting the so called Monodromy matrix, until the propagated trajectory is a periodic orbit. The initial guess is then incrementally changed until the desired orbit is obtained.
Once the best periodic approximation of the target orbit is computed, then we use the Monodromy matrix's eigenvalues to obtain the stable and unstable manifolds. The Monodromy matrix is obtained integrating the state transition matrix over an orbital period T. The state transition matrix is the matrix that linearly relates the perturbation of the initial ($\delta x(t_0)$) state with the perturbation of the state after a time t (Eq (4)).

$$\delta x(t) = \Phi(t, t_0) x(t_0) \tag{4}$$

where

$$\Phi(t, t_0) = \frac{df(x, t)}{dx}$$

The eigenvalues of the Monodromy matrix can be stable or unstable: the manifolds are natural converging - stable- or diverging - unstable, trajectories around the periodic orbit, according to the eigenvector directions of the stable (unstable) eigenvalues. They formally exist under the CR3BP.

Boundary conditions

The boundary conditions are those that the chaser's trajectory should match at the end of the phasing and they are reported in Table 2. The reference orbits are shown in Figure 3. To match the desired boundary conditions a stable manifold of the target orbit was selected at the aposelene - the furthest point of the orbit from the Moon - that guarantees the matching of the conditions and the convergence of the chaser towards the target avoiding collisions for a whole orbit.
The line in cyan in Figure 3 represents the resulting stable manifold that will take the chaser to the final desired conditions listed in the table. This is a stable manifold of the target's NRHO, which satisfies the collision - free requirements. Figure 4 shows that the passive safety is satisfied, and the selected manifold is collision - free. Passive safety was a mission requirement, with specified values of Keep Out Zones.

Table 2: Boundary Conditions for Phasing

Initial Orbit	Insertion Point
LLO Polar	near NRHO Aposelene
100 Km altitude	$>$ 50 Km below, $>$ 86 Km behind

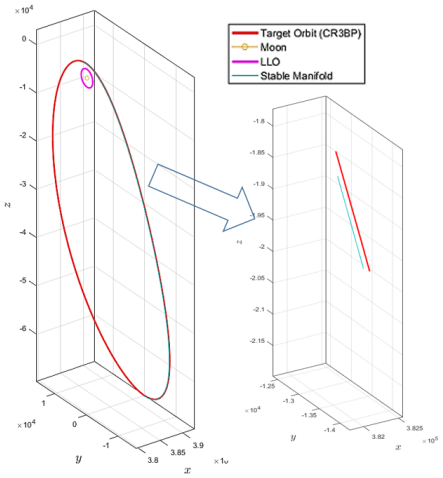

Figure 3: Reference Orbits for Phasing Design

PHASING DESIGN METHODS

Three different methods to design the phasing manoeuvre are proposed in this section. The first method is based on the Lambert's problem initial guess followed by a differential correction, the second method uses a Hohmann solution as initial guess and then uses the differential correction approach to get a good phasing manoeuvre, the third method is based on an optimisation approach.

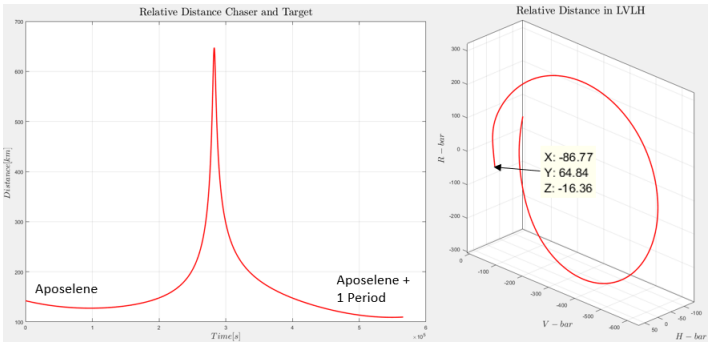

Figure 4: Relative Distance Chaser - Target on the stable Manifold

Direct Phasing using Lambert's initial Conditions and Two Body Dynamics

A classical procedure for determining an initial transfer velocity is given by the solution of the problem proposed by Lambert in the 18th century. It requires finding all possible trajectories (or the optimal trajectory) $\mathbf{r}(t)$ that connect an initial point $\mathbf{r}(t_1)$ at time t_1, with a final point $\mathbf{r}(t_2)$ at time t_2, under a gravitational field, and with the time of flight specified by the difference $TOF = t_2 - t_1$. For the two body case, the solution is known to provide two unique trajectories (long TOF and short TOF), which satisfy the boundaries [12], [13]. In the case of CR3BP or of a gravitational field generated by three or more masses, the problem does not have a simple solution, and numerical approximants are necessary to solve the associated boundary value problem. In addition, Lambert's problem usually has many different solutions in the three body environment for any specified initial data set (such as the terminal transfer positions, transfer time, and number of complete orbits around the attracting centre).
The computation of a first guess on the initial velocity is crucial, and can be done using the procedure in [1], with final position and final velocity written in terms of initial position, initial velocity for a given time of flight. Using the Lagrange coefficients f and g formulation, we have in fact:

$$\mathbf{r}(t_2) = f\mathbf{r}(t_1) + g\mathbf{v}(t_1) \tag{5}$$

$$\mathbf{v}(t_2) = \dot{f}\mathbf{r}(t_1) + \dot{g}\mathbf{v}(t_1) \tag{6}$$

from which we obtain:

$$\mathbf{v}(t_1) = \frac{1}{g}[\mathbf{r}(t_2) - f\mathbf{r}(t_1)] \tag{7}$$

$$\mathbf{v}(t_2) = \frac{1}{g}[\dot{g}\mathbf{r}(t_2) - \mathbf{v}(t_1)] \tag{8}$$

The Lagrange coefficients, which are functions of true anomaly, and time, and their time derivatives are computed as in [13] and [14], although more recent algorithms could also be used, such as those in [10], [15], [16], and [17].

Trajectory computation : Once a set of initial conditions are obtained, we fix a time of flight, and the trajectory is propagated using differential correction on the linearized dynamics to reach the final state. This procedure provides the system's transition matrix. The error on final position and the inverse of the transition matrix are used to correct the initial velocity value, and this procedure continues until the position at the final time is below the constraints specified above. To summarise the two impulse direct transfer phasing manoeuvre is designed in two steps:

- Step 1: determine a first guess on the departure velocity from the lunar orbit. This can be accomplished by solving a Lambert's problem or, as shown later, using a Hohmann transfer.

- Step 2: apply a differential correction propagation to correct the initial velocity, based on the boundary conditions at the final time, so that the spacecraft arrives at the final point with an acceptable error.

An example is shown in Figure 5. In the figure, the blue line corresponds to the trajectory evolution based on Lambert's theorem in the two body problem. The black line is the result of the differential correction propagation using the CR3BP model. The final position corresponds to an eccentric anomaly of 180 degrees. The time of flight is obtained from Lambert's theorem application using Eq. (5.3-12) from [13], or Eq. (5.39) from [1], and results in a value of 15.72 hours. Figure 6 shows the evolution of the trajectory propagated for

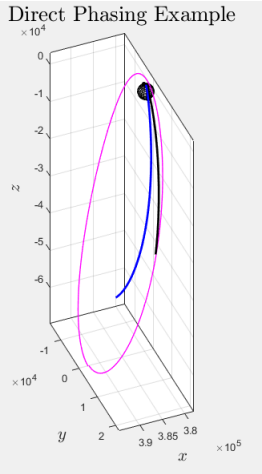

Figure 5: Example of direct Phasing using Lambert's Theorem

for different (longer) times of flight. 9 different TOF were used from 15.72 to 78.6 hours (0.655 - 3.275 days). The out-of-plane nature of the transfer orbits is evident from the simulations. Transfer trajectories propagated to the Aposelene region as final point, with different TOF are shown in Figure 7. Figure 8 shows a summary

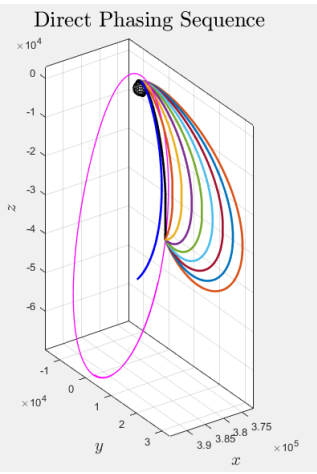

Figure 6: Phasing Trajectories: same End Point, Different TOF

of the tests carried out for the direct transfer using Lambert's first guess and the propagation via differential correction. The figure presents the results as function of different TOF and different final positions in the vicinity of the target orbit, combining what is described in the previous figures. The transfer trajectories were computed according to Table 3, where T is the target orbit period. The computation of the ΔV for the

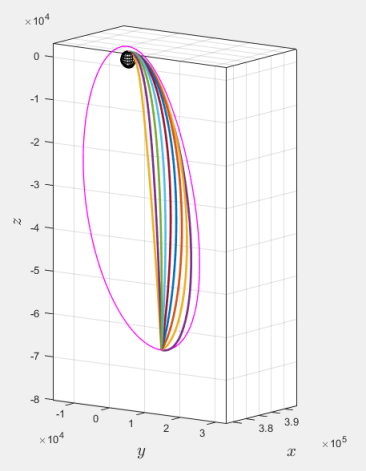

Figure 7: Phasing Trajectories: End Point at Aposelene, Different TOF

Table 3: Time of Flight and Final Point Location

Propagation time	True Anomaly
1.4T	152 deg.
1.35T	159 deg.
1.3T	163 deg.
1.25T	167 deg.
1.2T	170 deg.
1.15T	172 deg.
1.1T	175 deg.
1.05T	177 deg.
One T	180 deg.

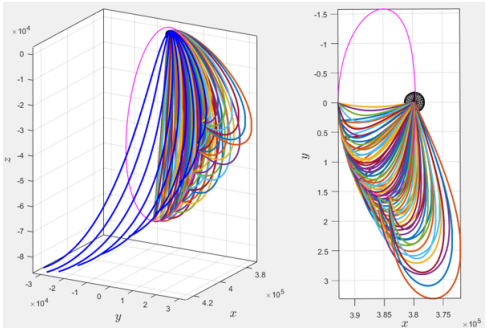

Figure 8: Phasing Trajectories: Summary Results

transfers shown above is performed assuming the manoeuvre to be obtained by two instantaneous impulses,

and by the relationship:

$$\Delta V = V(t_0) - V_{LLO} + V_{manifold} - V(t_0 + TOF) \tag{9}$$

The fuel expenditure depends on many factors. In this work, we related the ΔV to the stable manifold propagation time, and the time of flight, in order to obtain a general picture of the phasing requirements. The results are summarized in Figure 9. In the figure the x - axis represents the propagation time (in hours) of

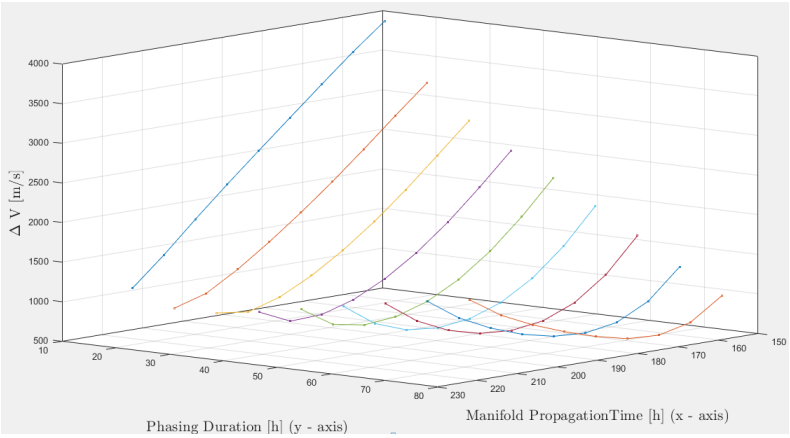

Figure 9: Direct Phasing Summary

the stable manifold from LLO to the final position location; the nine points show selected locations of the manifold starting from the aposelene. The y - axis represents the selected duration (in hours) of the phasing manoeuvre, and the z - axis shows the associated ΔV consumption computed according to Eq. (9). A total of 81 runs were performed, in order to create the grid in the figure.The total propagation time was selected to be about 62 hours.

Consider, for instance, the two-dimensional projections of Figure 9 shown in Figure 10. The point in the

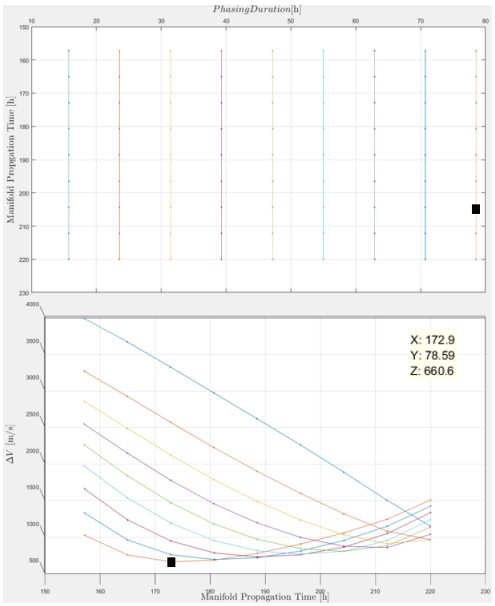

Figure 10: Phasing Duration and ΔV

figure indicates the amount of ΔV used for a direct phasing of 78.59 hours, with a manifold propagated at

time 180.8 hours. From the same figure we can also determine the minimum ΔV, which is about 660.6 m/s. Combining the results in Figures 8 and 9, we obtain the phasing trajectory, which produces the least expenditure in ΔV. This is shown in Figure 11.

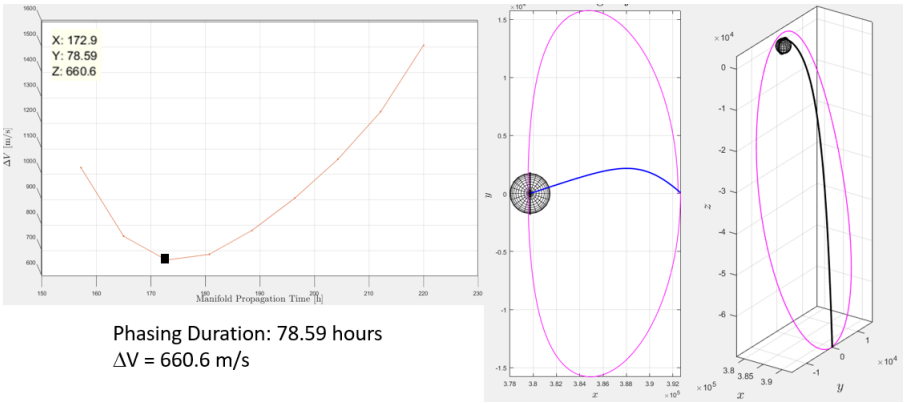

Figure 11: Direct Phasing with Lambert: Transfer Orbit and Fuel Expenditure

Direct Phasing using Hohmann Transfer initial Conditions

A second direct phasing analysis was performed using as initial guess the position determined by a standard Hohmann transfer technique. Only few significant cases are proposed for this approach, since the objective of this test was to understand if there was any advantage in terms of ΔV in changing the initial guess selection methodology.
Three phasing trajectories were computed for three different times of flight as multiples of the orbit period (T = 6.25 days). The results are shown in Figure 12. The times of flight and the associated ΔV are reported

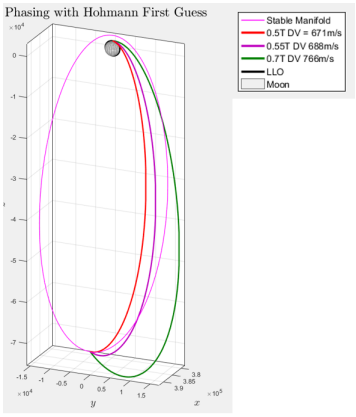

Figure 12: Phasing Trajectories using a Hohmann First Guess

in Table 4. The fuel consumption is higher than the one found before, for all times of flight, for this reason only three attempts were performed. The results shown in this section can be qualitatively compared with those in reference [3] Figure 5 (ΔV = 657 m/s), and [11] Table 3.3 (ΔV = 654.3). The ΔV needed for direct transfer is similar. Potential improvement can be obtained via optimization with multiple firing, and a more precise computation of the ΔV itself.

Table 4: Direct Phasing Summary using Hohmann

TOF	ΔV [m/s]
0.5 NRHO Period	671
0.55 NRHO Period	688
0.7 NRHO Period	766

Optimised Phasing Procedure

This section describes the work related to defining a phasing sequence via optimisation. A phasing trajectory is designed under the CR3BP dynamic model, based on critical parameters such as position error, ΔV, TOF, and number of impulses.
Consider the reference equations for the CR3BP model described by Eq. (2) or in compact form by Eq. (1). The approach used is the selection of an appropriate cost function, whose minimisation will produce a set of optimal manoeuvres. The optimization is based on the algorithms present in the $fmincon$ nonlinear programming solver available in Matlab^{TM} [18]. The general problem can be formulated as that of minimizing a cost function **J(x)** with respect to some state vector **x**, with constraints given by:

$$\begin{aligned} c(\mathbf{x}) &\leq 0 \\ c_{eq}(\mathbf{x}) &= 0 \\ A \cdot \mathbf{x} &\leq \mathbf{b} \\ A_{eq} \cdot \mathbf{x} &= \mathbf{b}_{eq} \\ lb \leq \mathbf{x} &\leq ub \end{aligned}$$

The function uses a gradient-based method that is designed to work with problems that are continuous, with at least continuous first derivatives. A sequential quadratic programming algorithm is used by $fmincon$ with updates of an estimate of the Hessian matrix at each iteration [19], [20]. In our problem, we chose a quadratic cost function given by a weighted sum of the position error and the ΔV. Its analytical expression is given by:

$$\mathbf{J} = q_1 \big\|\mathbf{e}\big\|^2 + q_2 (\sum_i \big\|\Delta V_i\big\|)^2 \tag{10}$$

The vector **e** is the error between final state and desired state,

$$\mathbf{e} = \mathbf{x}_{fin}^{Syn} - \mathbf{x}_{des}^{Syn}$$

and ΔV_i are the fuel consumption expenditures at each impulse. The weighting coefficients q_1 and q_2 are designer selection. In the following tests their numerical values were selected as in Table 5. In the optimization, the number of impulses (thruster firings) is fixed, and simulations were performed assuming the number of impulses equal to 2, 3, 4, and 5. Spacing of the firings as well as fuel expenditure between odd/even firings were a result of the optimization and its trade-off between position error and ΔV. The starting point was LLO, the arrival point was the aposelene of the target orbit and the selected stable manifold was maintained the same as in the previous section. The simulation results are summarized in Table 6. The graphical rep-

Table 5: Weighting Values in the Cost Function

Weight	Value
q_1	9×10^4
q_2	10

Table 6: Fuel Expenditure as Function of the Number of Impulses (Firings)

Number of Impulses	Total ΔV
2	661 m/s
3	709 m/s
4	688 m/s
5	717 m/s

resentation of the phasing trajectories in the case of 2 impulses and 4 impulses are shown in Figure 13. The two impulse case, although requires a smaller ΔV, has a very large position vector error. Based on the above

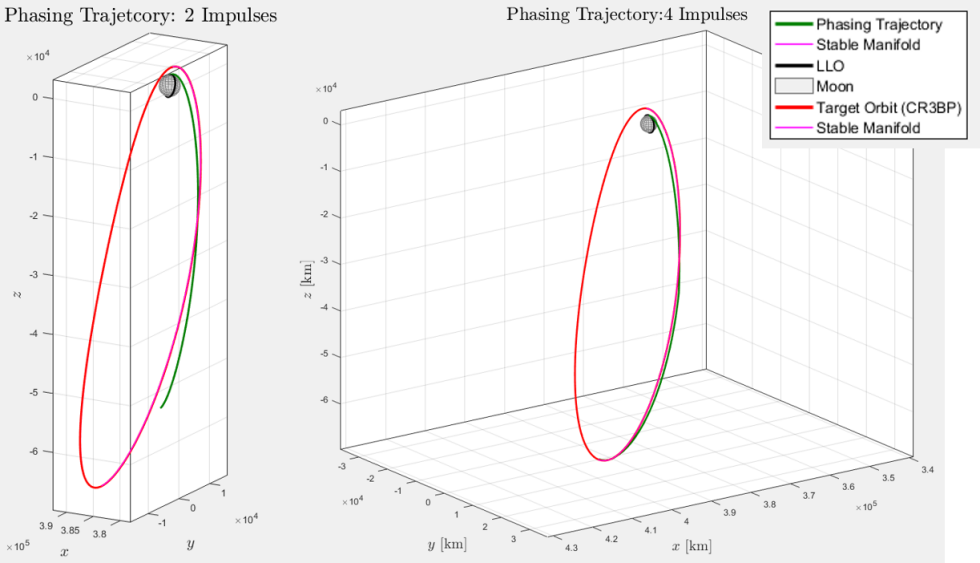

Figure 13: Multiple Impulse Phasing.Two and four impulse Cases

results, a four - impulse manoeuvre was selected, since it provided a lower position error than a 2 impulse case. The stable arrival manifold was changed by varying the value of the initial perturbation in the propagation (80 km in norm) along the direction of the eigenvector associated with the eigenvalue less than 1 of the Monodromy matrix, and used for the propagation of the manifold itself. The results are shown in Table 7. Figure 14 shows the trajectory corresponding to a four-impulse with the original initial perturbation (the same as the plot on the right in Figure 13) and that resulting from a 200 km perturbation. A change in manifold selection does not appreciatively change the fuel consumption. In order to verify potential ΔV reduction as a function of TOF, the phasing manoeuvre was propagated for five times the target orbital period. The selected trajectory was the one corresponding to the stable manifold generated with an initial perturbation of 100 km (see third row in Table 7). The longer propagation yields an arrival point closer to the target orbit propagated under the Ephemeris model. The simulation results are summarized in Table 8. Table 9 gives the results in terms of perturbation amount.

The resulting best scenario corresponds to a five period manifold propagation, with four impulses and a total expenditure of ΔV = 671 m/s. The phasing manoeuvre is shown in Figure 15. The total ΔV divided into the impulse occurrence is shown in Table 10. As in all cases tested, the largest ΔV occurs at the departure from LLO. If we propagate the phasing trajectory over a five-period time, however, the distance to the manifold increases to values that do not satisfy the specifications imposed by the boundary conditions defined above. An example is shown in Figure 16 for a manifold computed with a 100 km initial perturbation

Table 7: ΔV as Function of Manifold Selection

Perturbation (km)	Total ΔV
80 (original)	688 m/s
90	687 m/s
100	687 m/s
150	687 m/s
200	686 m/s

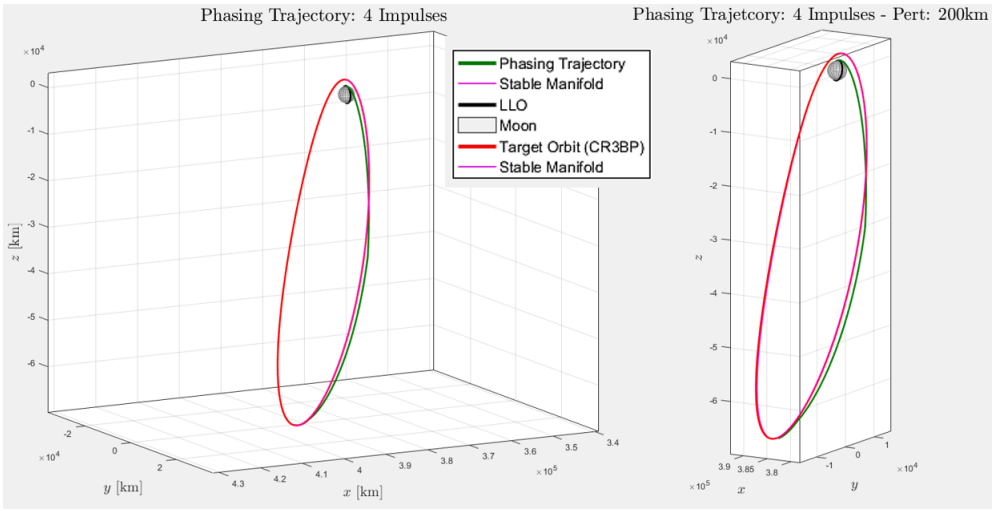

Figure 14: Phasing Trajectories with different Manifolds

Table 8: ΔV as Function of Phasing Duration

No. Impulses	100 km, 5P	100 km, 5.2P	100 km, 5.4P	
3	676 m/s	671 m/s	$>$ 700 m/s	
4 1045 m/s	**671 m/s** $>$ 700 m/s	754 m/s	height5	677 m/s

Table 9: ΔV as Function of Manifold Selection for 5*Period Propagation

Perturbation (km)	Total ΔV
80 (original)	673 m/s
90	672 m/s
100	**671 m/s**
150	674 m/s
200	682 m/s

Table 10: ΔV Consumption at each Impulse

Time of Flight ΔV	
T = 0	639 m/s
T = 1.19 day	32 m/s
T = 1.28 day	0.01 m/s
T = 2.2 day	0.05 m/s

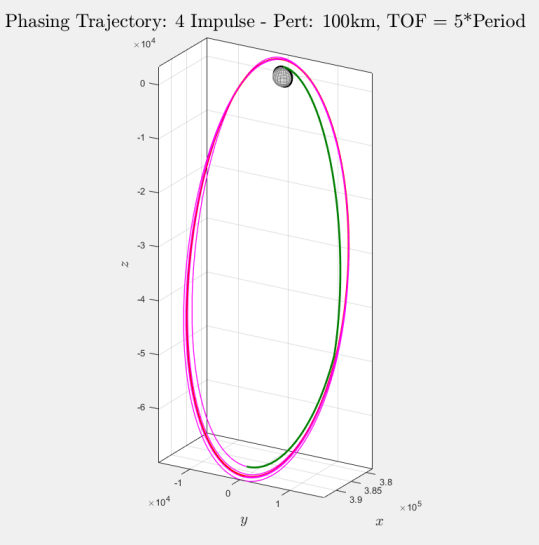

Figure 15: Phasing Trajectory Result: 32.8 Days Manifold Propagation

(projection on the $x - y$ plane). The increase in distance is evident already after 2 time periods. Note that similar results were obtained for the case of 80 km perturbation. To reduce the error between phasing and manifold, the optimization was performed by changing the weight of the error to: $q_1 = 9x10^6$. The simulation results are shown in Figure 17 for an initial perturbation of 100 km in the manifold propagation, and Figure 18 for an initial perturbation of 80 km in the manifold perturbation (in both cases the propagation was performed for 5 orbital periods). In both cases the final position error between the phasing trajectory and the the desired final position is lower that the one shown in Figure 16. Of course there is a slight increase on the the total ΔV.

In summary, the phasing trajectory that appears more promising is the one that reaches the target stable manifold generated with an initial perturbation of 80 km, and a propagation time of five time the target orbit period. The ΔV consumption, and the impulse timing are shown in Table 11. The main reasons for this choice are:

- The target manifold satisfies the requirements after a time of four periods, without additional manoeuvres, which are necessary for a 100 km initial perturbation,
- The position error is lower, although there is a slight increase in ΔV,
- The propagation to five orbital periods yields a phasing manoeuvre duration of about 29d 5h 2min before satisfying the insertion requirements. However, if we remove the CR3BP restriction and perform

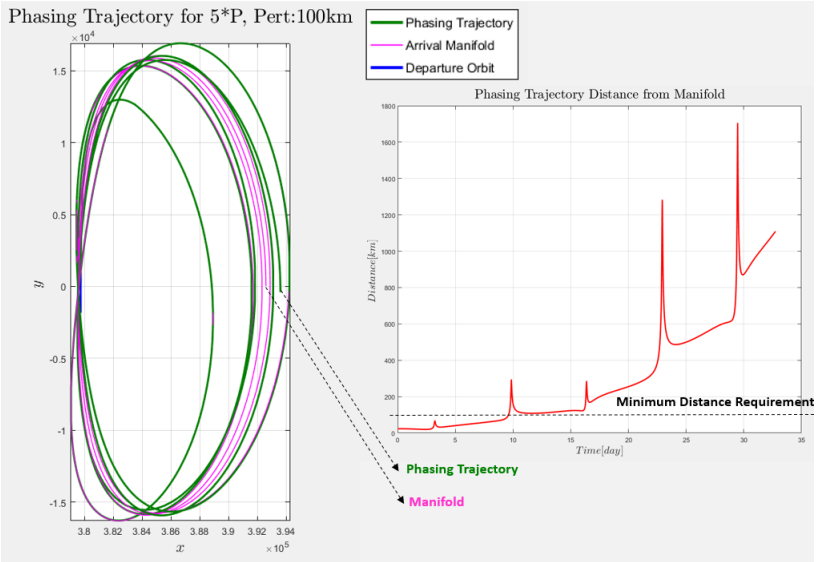

Figure 16: Phasing Trajectory Result, TOF = 32.8 Days

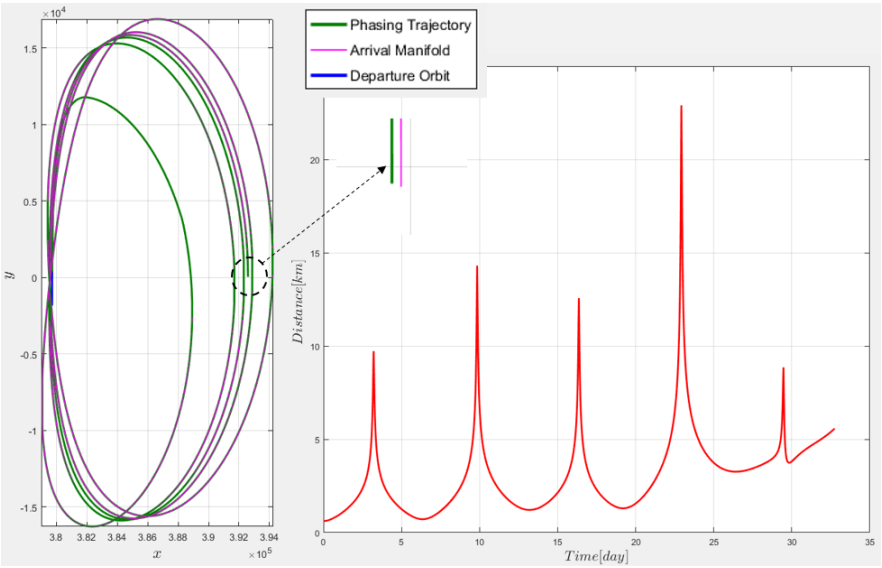

Figure 17: Phasing Trajectory Result, 100km Perturbation, higher Weight on Position Error

Table 11: ΔV Consumption at each Impulse

Time of Flight ΔV	
T = 0	639 m/s
T = 0.91 day	39.4 m/s
T = 1.638 day	0.001 m/s
T = 0.67 day	0.001 m/s

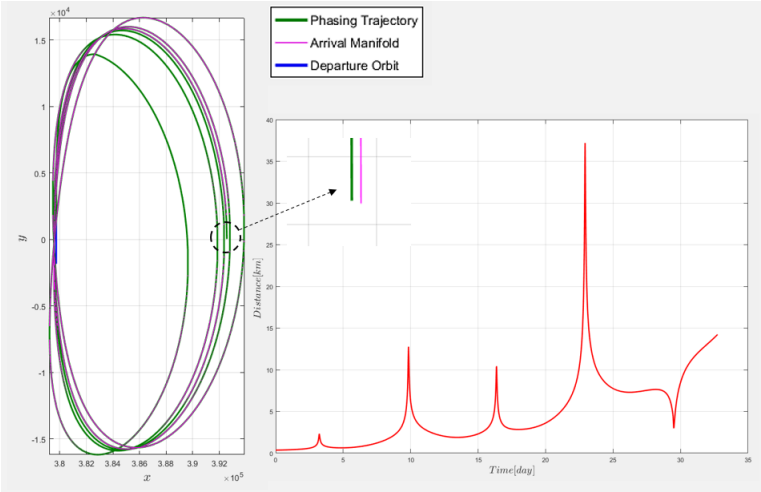

Figure 18: Phasing Trajectory Result, 80km Perturbation, higher Weight on Position Error

the targeting with the real LOP-G orbit, the final position on the manifold is much closer to the orbit, than the one period case,

- The real target orbit considered here was obtained using "Free-Flyer" code with propagation dates 09-Jan-2020 to 07-Feb-2020. This results in a more stable phasing compared to the one using the manifold obtained with a 100 km initial perturbation, if we use ER3BP equations (see later).

Note: direct targeting to the real orbit was not performed, since it would not provide any guaranteed stable drift to the target, unlike the stable manifold.

ELLIPTIC RESTRICTED THREE BODY PROBLEM VALIDATION

In order to validate the selected manoeuvre, the equations of motion were propagated using the ER3BP model. The complete equation set can be found in [21] section 4.2, and are summarized here for clarity's sake in the Synodic frame, assuming that its origin and the origin of the Inertial system coincide.

$$\begin{cases} \tilde{x} - 2\tilde{\omega}_{s/i}\tilde{y} - \tilde{\omega}_{s/i}\tilde{y} - \tilde{\omega}_{s/i}^2\tilde{x} = -(1-\mu)\dfrac{\tilde{x}-\tilde{R}_1}{\tilde{r}_1^3} - \mu\dfrac{\tilde{x}+\tilde{R}_2}{\tilde{r}_2^3} & \text{(11a)} \\ \tilde{y} + 2\tilde{\omega}_{s/i}\tilde{x} + \tilde{\omega}_{s/i}\tilde{x} - \tilde{\omega}_{s/i}^2\tilde{y} = -(1-\mu)\dfrac{\tilde{y}}{\tilde{r}_1^3} - \mu\dfrac{\tilde{y}}{\tilde{r}_2^3} & \text{(11b)} \\ \tilde{z} = -(1-\mu)\dfrac{\tilde{z}}{\tilde{r}_1^3} - \mu\dfrac{\tilde{z}}{\tilde{r}_2^3} & \text{(11c)} \end{cases}$$

where *normalized gravitational parameter* $0 < \mu < 0.5$, for the case of $M_1 > M_2$ is given by:

$$\mu = \frac{\mu_2}{\mu_1 + \mu_2} = \left(1 + \frac{M_1}{M_2}\right)^{-1} \implies \quad \mu_2 = \mu, \quad \mu_1 = 1 - \mu \tag{12}$$

with $\tilde{(.)}$ indicating the non-dimensional value.
The objective of this computation was primarily a verification, at the simulation level, of potential divergence of the phasing over the five period time. The simulation shows that the phasing appears possible under the elliptic motion, although the trajectory diverges after 6 orbits for the 100 km perturbation manifold, and 7

orbits for the 80 km perturbation manifold. A graphical representation for the 80 km manifold perturbation is shown in Figure 19.

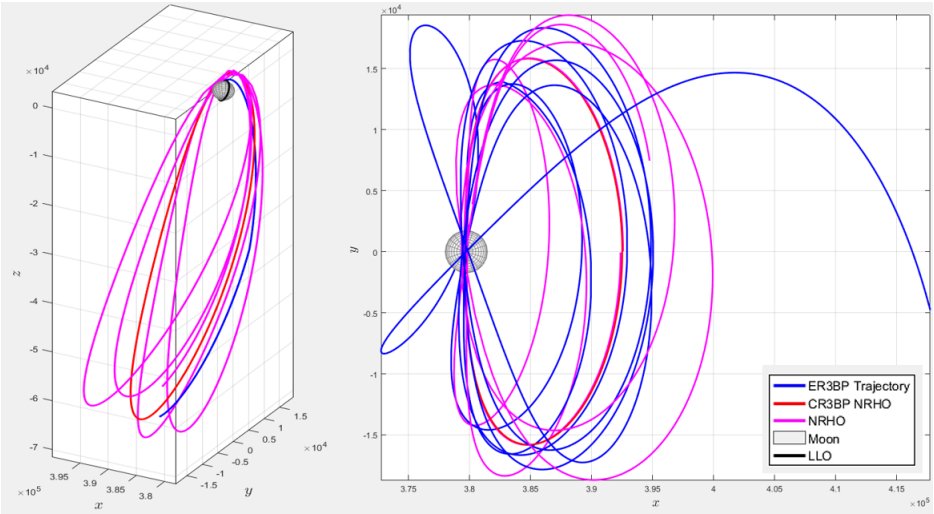

Figure 19: Phasing Trajectory, 80 km Perturbation, ER3BP Propagation

Additional tests were performed to verify potential improvement on the the selected trajectory. The first test was to take the trajectory shown in Figure 15 and Table 10 and perform a differential correction algorithm, instead of changing the weight on the error position and perform a new optimization. The trajectory is shown in Figure 20. The connection to the manifold is achieved at the expense of an additional fuel expenditure, bringing the total to ΔV = 744 m/s instead of the original 671 m/s and 682 m/s obtained with the optimization procedure.

The second test was to perform an optimization using the cost function in Eq. (10) with weights q_1 =

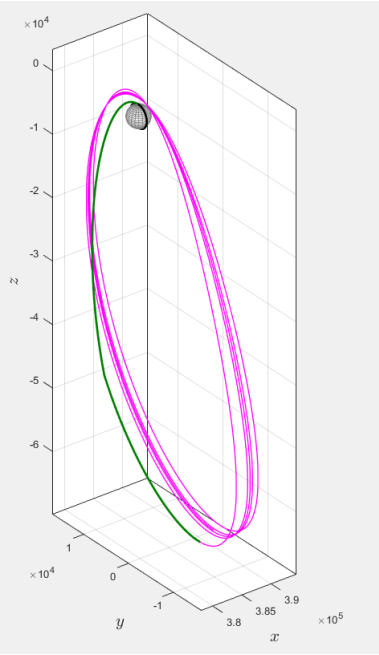

Figure 20: Phasing Trajectory with Differential Correction, 100 km Perturbation, ER3BP Propagation

$9x10^6$, and q_2 = 10, but using the ER3BP model. This serves as a comparison with the propagation that uses the CR3BP model, whose results were shown in Figure 15, and in the third row of Table 9. The phasing manoeuvre is computed for a one half of the target orbital period and for a time of flight of five times the period. The results are comparable in terms of position error; the manoeuvre, however, requires a total ΔV = 703 m/s, as compared to ΔV = 671 m/s, for the circular restricted model propagation. In addition, the optimization algorithm takes a much longer time to converge. The phasing trajectory is plotted in Figure 21, where on the left the phasing trajectory is shown for a half period TOF, and on the right for a TOF of five orbits.

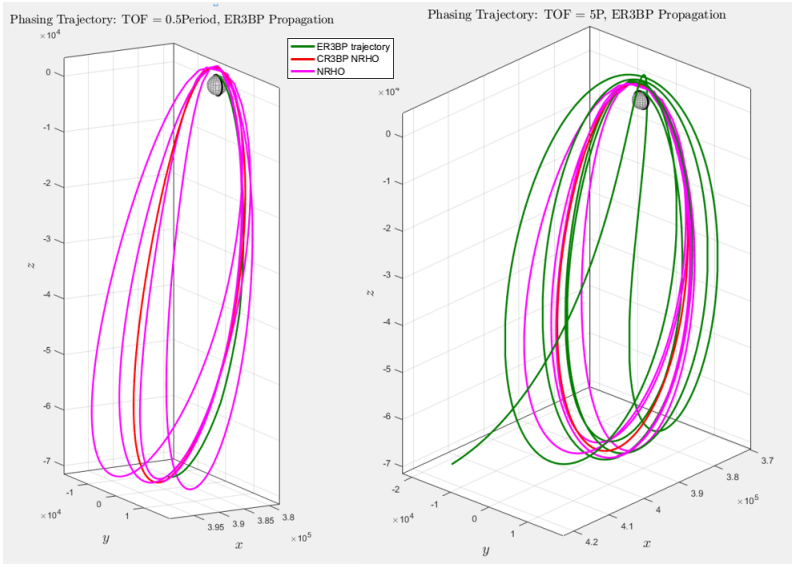

Figure 21: Phasing Trajectories with ER3BP Equations: 0.5P (left), 5P (right) Propagation

Comments on ΔV Expenditure

All previous results have shown that the main contributor to the total ΔV is the amount required for departing LLO. This is due to the high orbital speed of the chaser, while orbiting at an altitude of 100 km from the surface of the Moon.
The situation improves if we consider LLO parking orbits at a higher altitude. For instance, when a LLO is considered at an altitude of 200 km, the total ΔV reduces to 655 m/s. This fact needs to be considered at the mission design phase, in order to optimise the total budget for the mission. Figure 22 describes a sample phasing with a one half period TOF, leaving LLO at 200 km altitude. The target manifold is computed with a 100 km perturbation, and propagated for five times the orbital period.

COMPARISON AND CONCLUSIONS

In this paper an analysis of phasing trajectories was performed, and the results evaluated in terms of ΔV expenditures, time of flight, and position errors achieved at the final time.
The study of phasing considered direct transfer from LLO to the target orbit using two - impulse manoeuvres with initial conditions computed from a two body Lambert's approach, from a direct Hohmann transfer, and a gradient-based optimization with multiple impulses. The resulting transfer trajectory was injected into a stable manifold generated by the target orbit, and selected in the direction of the eigenvector associated to the relevant eigenvalue of the appropriate Monodromy matrix.
A summary of the results is shown below, with reference to the three phasing approaches.

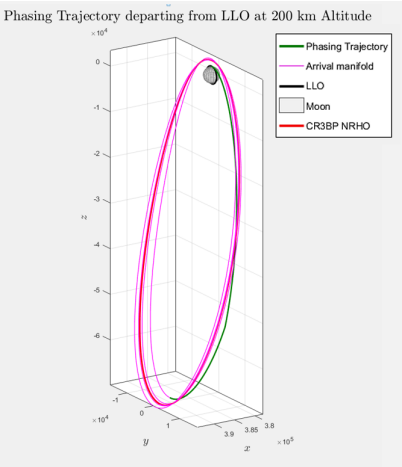

Figure 22: Phasing Trajectory for higher LLO Altitude

Summary and Comparison

1. *Lambert, two-impulse*

   - The boundary conditions needed to solve the problem are computed using Lambert's approach.
   - The stable manifold is computed via propagation from an 80 km perturbation and it is met at the aposelene. The final position error is zero, since we are on the desired manifold.
   - the time of flight of the phasing trajectory is 78.5 hours (half period of the target orbit).
   - The total expenditure is $\Delta V = 660$ m/s.
   - The phasing trajectory is shown in Figure 11, and it is a full out-of-plane path. This is why this approach may result in an increased fuel expenditure. To be noted is the fact that the orientation of the LLO orbit was not specified, thus the amount of out-of-plane imposed by Lambert could change.

2. *Hohmann, two-impulse*

   - The boundary conditions needed to solve the problem are computed using a standard Hohmann approach.
   - The stable manifold is computed via propagation from an 80 km perturbation and it is met at the aposelene. The final position error is zero, since we are on the desired manifold.
   - The time of flight is similar to the previous case (half period of the target orbit).
   - The total expenditure is $\Delta V = 671$ m/s.
   - The phasing trajectory is shown in Figure 12.

3. *Multiple impulse optimization*

   - The optimization procedure does not use differential correction, thus it produces position errors at the final time, which depend on propagation equations and optimization stopping conditions.
   - A different number of impulses was evaluated, with the best results obtained for a 4-impulse sequence (see Table 5).
   - Different stable manifolds were evaluated in terms of ΔV expenditure (see Table 7). The computed ΔV are 688 m/s and 687 m/s for a manifold propagation of one orbital period (80 km and 100 km perturbations).

- The phasing trajectory time of flight is half orbital period and it is shown in Figure 14.
- Improvement in the final position error and ΔV can be obtained by longer manifold propagation, and longer time of flight of phasing trajectory. In particular, a five period manifold propagation, and a phasing trajectory time of flight of 29d 5h 2min yield a position error within the requirements ad a ΔV = 678.401 m/s, as shown in Figure 18.

4. *ER3BP Propagation*

   - Phasing trajectory time of flight of half period, ΔV = 703 m/s, see Figure 21.

The results show a similar ΔV consumption for all tested procedures. Improvement on the results are suggested based on extensive simulation campaign, which is outside the scope of the present activity.

REFERENCES

[1] H. D. Curtis, *Orbital mechanics for engineering students*. Butterworth-Heinemann, 2013.

[2] B. A. Sukhanov A. and P. A., "Lambert Problem Solution in the Hill Model of Motion," *Celestial Mechanics*, Vol. 90, No. 6, 2004, pp. 331–354.

[3] L. Bucci, M. Lavagna, F. Renk, *et al.*, "Phasing and rendezvous operations on non-Keplerian orbits in the Earth-Moon system," *69th International Astronautical Congress (IAC 2018)*, 2018, pp. 1–8.

[4] H. Shang, S. Wang, and W. Wu, "Design and optimization of low-thrust orbital phasing maneuver," *Aerospace Science and Technology*, Vol. 42, 2015, pp. 365–375.

[5] M. R. Gomez G Llibre J and S. C, *Dynamics and Mission Design Near Libration Points. Vol I. Fundamentals: The Case of Collinear Libration Points*. World Scientific Monograph Series: Mathematics, 2001.

[6] W. S. Koon, M. W. Lo, J. E. Marsden, and S. D. Ross, "Dynamical systems, the three-body problem and space mission design," *Differential Equations 1999: (In 2 Volumes)*, pp. 1167–1181, World Scientific, 2000.

[7] L. Bucci, M. Lavagna, F. Renk, *et al.*, "Relative dynamics analysis and rendezvous techniques for lunar Near Rectilinear Halo Orbits," *68th International Astronautical Congress (IAC 2017)*, Vol. 12, International Astronautical Federation, IAF, 2017, pp. 7645–7654.

[8] E. Blazquez, L. Beauregard, and S. Lizy-Destrez, "Safe natural far Rendezvous approaches for Cislunar Near Rectilinear Halo Orbits in the Ephemeris model," 2018.

[9] *Near rectilinear orbits around the moon as operational orbit for the future deep space gateway*, Oberpfaffenhofen, Germany, 2016.

[10] E. Blazquez, L. Beauregard, and S. Lizy-Destrez, "Optimized Transfers between Eart-Moon Invariant Manifolds," *7th ICATT Conference*, ESA, 2016, pp. 1–9.

[11] ESA, "Lunar Ascent Element, Human Enabled Robotic Architecture and Capabilities for Lunar Exploration and Science, Heracles, framework, ESA-HSO-K-TN-0011," 25/08/2017.

[12] K. Alfriend, S. R. Vadali, P. Gurfil, J. How, and L. Breger, *Spacecraft formation flying: Dynamics, control and navigation*, Vol. 2. Elsevier, 2009.

[13] R. R. Bate, D. D. Mueller, and J. E. White, *Fundamentals of Astrodynamics*, Vol. 2. Dover, 1971.

[14] V. R. Bond and M. Allman, *Modern Astrodynamics: Fundamentals and Perturbation Methods*, Vol. 2. Cambridge University Press, 1996.

[15] I. D., "Revisiting Lambert's problem," *Celestial MEchanics and Dynamical Astronomy*, Vol. 121, No. 1, 2015, pp. 1–15.

[16] Y.-Z. Luo, "Quantitative Performance for Spacecraft Rendezvous Trajectory Safety," *Journal of Guidance, Control, and Dynamics*, Vol. 34, No. 4, 2011, pp. 1264–1269.

[17] Y.-z. Luo, L.-b. Liang, Z.-y. Niu, and G.-j. Tang, "Safety-optimal linearized impulsive rendezvous with trajectory uncertainties," *Journal of Aerospace Engineering*, Vol. 27, No. 6, 2013, pp. 431–438.

[18] ANON., *Optimization Toolbox*, Vol. 2. The Mathworks Inc., 2019.

[19] R. H. Byrd, "A Trust Region Method based on interior Point Techniques for Nonlinear Programming," *Mathematical Programmings*, Vol. 89, No. 1, 2000, pp. 149–185.

[20] M. J. Powell, *A Fast Algorithm for Nonlinearly Constrained Optimization Calculations*, Vol. 630. Springer-Verlag, 1978.

[21] M. G. Franzini, "Simulation tool for rendezvous and docking in high elliptical orbits with third body perturbation: Final Report," *ESA Contract No. 4000121575/17/NL/CRS/hh*, 20/02/2018.